Combined Calcination, Sintering and Sulfation Model for $CaCO_3$-SO_2 Reaction

Suhas K. Mahuli, Rajeev Agnihotri, Raja Jadhav, Shriniwas Chauk, and L.-S. Fan
Dept. of Chemical Engineering, The Ohio State University, Columbus, OH 43210

A mathematical model developed accounts for the multiple rate processes involved in the reaction of solid $CaCO_3$ or $Ca(OH)_2$ with SO_2 at high temperatures in the combustion environment. The model, based on the grain-subgrain concept, considers the concomitantly occurring calcination, sintering and sulfation reactions and their interactive effects on pore structure and reaction kinetics. It incorporates internal diffusion, reaction, and product layer diffusion in simulating the calcination of the $CaCO_3$ grain and subsequent sintering and sulfation occurring on the CaO subgrains. It is the first sulfation model to incorporate the true mechanism of diffusion through the solid product phase: the solid-state ionic diffusion of Ca^{2+} and O^{2-} ions in a coupled manner through the nonporous $CaSO_4$ (Hsia et al., 1993, 1995). Its predictions are compared with the random pore model (Bhatia and Perlmutter, 1981a) and the grain model (Szekely and Evans, 1971) using experimental CaO sulfation data from the literature as well as short-contact-time $CaCO_3$ and $Ca(OH)_2$ sulfation data reported previously. Mahuli et al. (1997) discussed a high reactivity modified calcium carbonate synthesized by optimizing the pore structural properties. This modified $CaCO_3$ can convert 70−75% of sulfation within 0.5 s, which is substantially higher than any other sorbents reported for similar particle size and reaction conditions. The model is used to predict the calcination and sulfation kinetics, as well as to simulate the surface area evolution of the modified $CaCO_3$, which provides further insights into its exceptional reactivity.

Introduction

The interaction of $CaCO_3$ or $Ca(OH)_2$ powder with SO_2 in the combustion environment at high temperatures has been the subject of numerous experimental kinetic studies as well as theoretical modeling efforts (Hartman and Coughlin, 1976; Bhatia and Perlmutter, 1981b; Simons and Garman, 1986; Alvfors and Svedberg, 1988, 1992; Silcox et al., 1989; Milne et al., 1990a,b,c). The problems associated with the loss in solids reactivity and incomplete conversion have also been extensively discussed (Borgwardt, 1970; Borgwardt and Bruce, 1986; Simons and Garman, 1986; Milne and Pershing, 1987; Ghosh-Dastidar et al., 1995, 1996). The SO_2 removal process at high temperatures (800−1,100°C) takes place through two reaction steps: calcination (decomposition) of the sorbent to produce high surface area and high porosity CaO, and reaction of CaO with SO_2 (sulfation) in the presence of O_2 to form the higher molar volume solid product, $CaSO_4$

$$Ca(OH)_2 \leftrightarrow CaO + H_2O \quad (1)$$

$$CaCO_3 \leftrightarrow CaO + CO_2 \quad (2)$$

$$CaO + SO_2 + \frac{1}{2}O_2 \leftrightarrow CaSO_4 \quad (3)$$

The sintering of CaO is a concomitant deactivation phenomenon which reduces the available surface area and porosity for the sulfation reaction. There are a number of factors which play a crucial role in determining the reaction rate and the overall solids conversion. In addition to particle size, the

Correspondence concerning this article should be addressed to L.-S. Fan.

sintering of CaO and its pore properties are critical for the overall sulfation behavior. Previous attempts at improving sorbent reactivity focused on either reducing the CaO particle size or modifying the $Ca(OH)_2$ with structural or chemical promoters to increase its surface area. For particles in the range of 1–5 μm, size does not play a determining factor in the overall reactivity (Milne et al., 1990c; Ghosh-Dastidar et al., 1996). Promoted hydrates with high surface area also did not exhibit significant improvements (Kirchgessner and Jozewicz, 1989). Ultrafine CaO of size < 0.1 μm produced by laser ablation has been shown to possess very high reactivity (Sadakata et al., 1994), but there are associated problems of particulate matter handling and control. The CaO sintering rate is strongly influenced by the initial sorbent type and the impurities in the solid (Borgwardt, 1989). Ghosh-Dastidar et al. (1996) have shown that the CaO derived from carbonate (c-CaO) sinters at a slower rate than hydroxide-derived CaO (h-CaO), but the pores of c-CaO derived from nonporous carbonate lie predominantly in the less than 50 Å size range which are susceptible to pore blockage and premature termination of sulfation reaction. Equally important is the pore-size distribution of the parent sorbent and that of the reactant CaO. They showed that a calcium carbonate with an open initial pore structure could yield higher sulfur capture than the hydrate sorbent particles.

Mahuli et al. (1997) have discussed the synthesis of a high reactivity $CaCO_3$, which reaches a conversion of more than 70% compared to about 30–35% for the commercial sorbents. The high reactivity calcium carbonate powder with high surface area and pore volume is produced by carbonation-precipitation of a calcium hydroxide suspension in a slurry bubble column reactor in the presence of a small amount of dispersing agent. The operating parameters of the reactor are optimized to generate carbonate particles of desired pore structural properties. They compared the sulfation characteristics of this modified carbonate (MC) with a commercial Linwood carbonate (LC) and a modified calcium hydroxide (MH). In spite of the pore properties of MH and MC being similar, the modified carbonate reactivity is much higher than the MH. Using pore structure evolution studies and its effects on reaction kinetics at short-contact times of less than 100 ms, Mahuli et al. (1997) elucidated the reasons for high reactivity of the modified carbonate. They showed that at the reaction conditions of interest here, an optimum pore-size range exists between 50–200 Å, which provides sufficient surface area for the sulfation reaction without causing rapid pore filling and pore-mouth plugging. Hence, the relative advantage of one sorbent over another may be caused by one or more of these important chemical and structural parameters. An effective sorbent should meet the necessary criteria of slow sintering rate, small particle size, and a favorable pore-size structure.

Modeling

Many gas-solid reaction models exist in the literature which have been used to predict the sulfation of precalcined and presintered CaO, as well as $Ca(OH)_2/CaCO_3$ sulfation. In modeling $CaCO_3/Ca(OH)_2$ sulfation, such models assume instantaneous calcination and negligible sintering. Wen and Ishida (1973), Pigford and Sliger (1973), and Hartman and Coughlin (1976) represent some of the earliest attempts of applying the grain model to sulfation data (Szekely and Evans, 1976). Fan et al. (1984) utilized a volume reaction model to account for the heterogeneous sulfation reaction of calcined limestone or dolomite. Hartman and Coughlin (1976) introduced the concept of residual porosity in order to predict ongoing sulfation even after the theoretically predicted porosity of the particle has been reduced to zero. Borgwardt and Bruce (1986) and Bruce et al. (1989) applied the limiting case of product layer diffusion control with the grain model to fit the CaO sulfation data. A number of researchers have modified the original grain model to account for structural changes either empirically or through theoretical considerations. Georgakis et al. (1979) modified the grain model by manifesting the lost particle porosity as an increase in grain size with reaction. Ranade and Harrison (1979, 1981) also modified the constant property grain model to account for both the sintering and reaction. They suggested that the role of sintering could be depicted as coalescence of grains to form bigger grains. Grain models based on overlapping grains have been developed for sulfation. Lindner and Simonsson (1981) and Alvfors and Svedberg (1992) developed their partially sintered spheres (PSS) model and applied it to CaO sulfation data. Sotirchos (1987), Sotirchos and Yu (1988), and Milne et al. (1990a,b) also developed models based on overlapping grains.

Pore models have been developed and used by many researchers to match CaO sulfation data (Ramachandran and Doraiswamy, 1982). The random pore model (Bhatia and Perlmutter, 1980, 1981a,b) takes into account the changes in pore structure due to formation of solid product and considers the overlapping and intersections among the pores. They introduced a pore structure parameter which is related to the effective grain shape factor proposed in the grain models (Szekely and Evans, 1971; Calvelo and Smith, 1971). They fitted their model to experimental CaO sulfation data of Borgwardt (1970) and Hartman and Coughlin (1976). Christman and Edgar (1983) developed a distributed pore-size model which takes into account the reaction and structural changes in pores of all the sizes. Applying sulfation data from Ulerich et al. (1977), their model is able to predict that the kinetic behavior of different calcined limestones is attributed to differences in their pore structures. Sotirchos and Zarkantis (1993) developed a structural model for CaO sulfation behavior with structural changes due to sulfation without considering the effects of sintering. In their model they conceptualized the porous structure to be a network of pores of distributed size and length. A number of other sulfation models have been proposed in the literature that consider the porous structure of the solid as a tree structure (Simons and Garman, 1986; Simons et al., 1987), as a Bethe network based on the concept of percolation (Reyes and Jensen, 1987) or as a Voronoi tessellation of polyhedra (Li et al., 1995).

Comprehensive $Ca(OH)_2/CaCO_3$ sulfation modeling has been attempted by some researchers. Alvfors and Svedberg (1988) modeled the overall sulfation of the $Ca(OH)_2$ particle by modifying their PSS model. They assumed first-order kinetics for the calcination surface reaction, and modeled sintering on the basis of German and Munir's (1976) work. Calcination and sintering were taken together to predict the surface area available for the sulfation. Pore diffusion, product

layer diffusion, and chemical reactions were considered for the sulfation step. Milne and Pershing (1988) presented a combined model using a grain model for sulfation, second-order kinetics for the sintering, and an empirically modified shrinking-core model for calcination. Milne et al. (1990a,b) applied the PSS model to simulate calcination, sintering, and sulfation of $CaCO_3$ particles. They assumed the sulfation reaction to be limited by product layer diffusion and diffusion of SO_2 through the pores. In their model sintering is defined as a function of surface area and takes into account the presence of CO_2 and H_2O on sintering.

Product layer diffusion (PLD)

Bhatia and Perlmutter (1981b) were the first to postulate (from fitting their model to the CaO sulfation data) that the product layer diffusion of SO_2 might be occurring via a solid-state diffusion mechanism. They further postulated formation of charged species on the surface of $CaSO_4$ by SO_2 and O_2 and inward movement of sulfate ions through the product layer with reaction at the $CaO/CaSO_4$ interface. Borgwardt et al. (1987) determined the effects of impurities on the reaction rate of CaO sulfation. They observed lower product layer diffusivities and slower reaction rates for pure CaO as compared to CaO doped with impurities. On the basis of these observations, they concluded that the diffusion process through the product layer involves ion transport with inward diffusion of SO_4^{2-} ions through the product layer. There exist other models in the literature which attempt to use crystallization thermodynamics in explaining the formation of the product layer. Duo et al. (1994) proposed a crystallization and fracture mechanism in which the solid product is formed in clusters of molecules or nuclei of a certain initial size. The initial critical size of nuclei dictates the structure of the product layer and its thickness. Duo et al. (1994) were able to predict the existence of a maximum thickness of product layer mathematically and explain incomplete conversion of Ca-sorbents with SO_2.

Hsia et al. (1993, 1995) used inert marker and reactive isotope experiments to clearly illustrate that the reaction front is not at the CaO-$CaSO_4$ interface, but at the $CaSO_4$/gas interface. They demonstrated that the ionic diffusion phenomenon involves in part the outward migration of Ca^{2+} ions (and O^{2-} in a coupled manner to satisfy local mass and charge balances) through the $CaSO_4$ product layer instead of inward SO_4^{2-} ion movement. The rhombohedral crystal structure of $CaSO_4$ has large tetrahedra of complex SO_4^{2-} ions with Ca^{2+} wedged in between. Further, the size of SO_4^{2-} ions is large compared to the Ca^{2+} ions, roughly 4.5 Å vs. 1.8 Å. As a result, the Ca^{2+} ions should inherently possess a higher mobility than the SO_4^{2-} ions. In order to explain the associated O^{2-} transport, Hsia et al. (1993) reasoned that the dissolution of CaO in $CaSO_4$ creates vacancies on some of the O^{2-} sites in the tetrahedra, thereby enhancing the mobility of O^{2-} ions, which are known to possess high mobility in the zircon-type lattice structure of $CaSO_4$ (Evans, 1964; Hsia et al., 1995).

In this study, the development of a combined mathematical model describing the simultaneous calcination, sintering and sulfation phenomena for small $CaCO_3/Ca(OH)_2$ particles is discussed. The model is based on the concept of grain-subgrain and includes first-order calcination kinetics, the structural changes due to thermal and CO_2/H_2O-aided sintering, and sulfation reaction. The model incorporates the actual mechanism of product layer diffusion as proposed by Hsia et al. (1993, 1995). The model is used to predict the sulfation and calcination data for the high reactivity $CaCO_3$, which exhibits more than 70% solids conversion. The model is tested with experimental calcination and sulfation data of other researchers. The detailed development of the modified $CaCO_3$ (MC) and its experimental short-contact time sulfation kinetics have been discussed elsewhere (Mahuli et al., 1997). The sulfation and calcination behavior of the calcium-based sorbent particles is studied in a specially designed isothermal high-temperature, entrained flow reactor (EFR) described elsewhere (Raghunathan et al., 1992, 1993; Ghosh-Dastidar et al., 1995). The EFR is shown in Figure 1. The EFR is capable of measuring the residence time of particles on-line using an optical guide assembly, and the water-cooled injection and collection probes accomplish instantaneous heatup and quenching of particles for time-resolved kinetic data acquisition. The reactor is operated in the differential mode with respect to the gas-phase SO_2 concentration, and the particle separation and classification is conducted *in-situ*. The overall gas-flow rate during sulfation is maintained at 15 slpm. The reactant gas consists of 3,900 ppmv SO_2, 5.46 vol. % O_2, and balance N_2 with trace amounts (less than 10 ppmv) of CO_2 and H_2O.

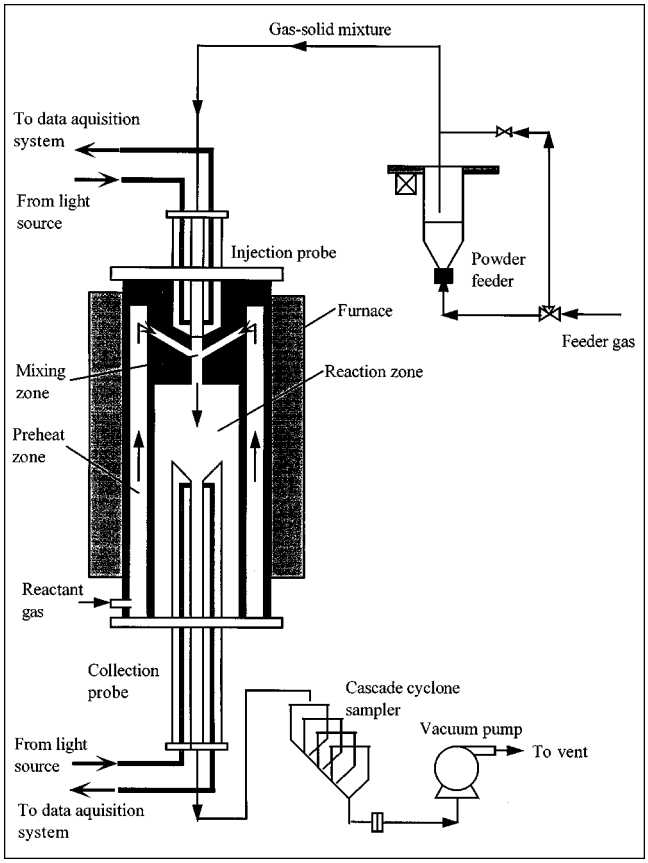

Figure 1. High-temperature EFR system.

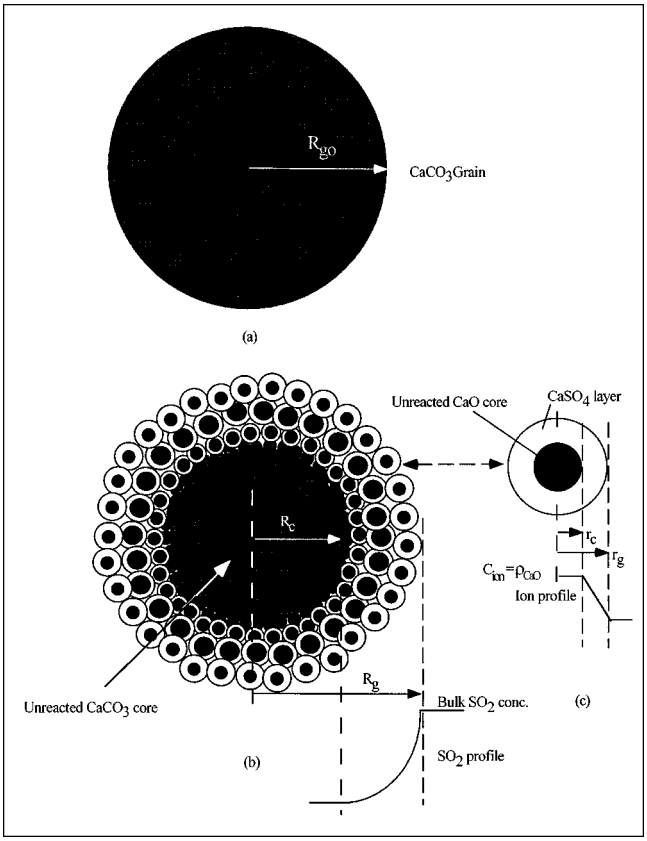

Figure 2. Combined grain-subgrain model.

(a) Single, spherical $CaCO_3$ grain; (b) partially calcined and sulfated grain with inner unreacted core and partially sintered and sulfated CaO subgrains; (c) partially sulfated CaO subgrain.

Combined Calcination, Sintering and Sulfation Model

The overall concept of the model is illustrated in Figure 2 and is applicable to either $CaCO_3$ or $Ca(OH)_2$. The following discussion and development of model equations are for $CaCO_3$; it can be extended to $Ca(OH)_2$ with the relevant modifications. A single $CaCO_3$ particle is assumed to be composed of identical, spherical, and nonoverlapping grains (Figure 2a). All the grains are considered to be at the same conditions of temperature and gas concentration. Calcination takes place on a single grain according to the sharp interface model. As $CaCO_3$ decomposes, subgrains of CaO are formed surrounding the unreacted $CaCO_3$ grain core. The CaO subgrains simultaneously undergo sintering and sulfation. The CO_2 diffuses out from the $CaO/CaCO_3$ interface to the grain surface, and the SO_2 diffuses inward through the voids between the subgrains. A subgrain could be partially sulfated or a newly formed CaO subgrain (Figure 2b). Ca^{2+} and O^{2-} ions diffuse outwards through the nonporous layer of $CaSO_4$ surrounding the CaO subgrains (Hsia et al., 1993) to react with SO_2 at the outer surface of the subgrain (Figure 2c). The shell surrounding the inner $CaCO_3$ core is composed of CaO subgrains of varying ages with varying degrees of sintering and sulfation. The most recently formed CaO layer, which surrounds the uncalcined sorbent core, possesses the highest surface area and porosity and would be least sintered and sulfated; whereas, the outermost layer would have the lowest surface area and would be highly sulfated. The partially sulfated sintering CaO offers resistance to the transport of both CO_2 and SO_2. At any given time depending on the radial position of the subgrain, the thickness of the $CaSO_4$ layer surrounding the subgrain would vary. The concentration profile of the Ca^{2+} and O^{2-} ions inside the subgrain is strongly dependent on the $CaSO_4$ layer thickness and SO_2 concentration at the subgrain surface.

Heat transfer is strongly dependent on the particle size, and, for large particles, it could impede the overall reaction rate. This model further assumes that there are no intraparticle or intragrain heat-transfer limitations. For small particles less than 5 μm in size, heatup and quenching have been shown to be extremely fast (Gullett et al., 1988; Alvfors and Svedberg, 1992; Mahuli et al., 1997). Detailed heat balance calculations considering convection from bulk gas, radiation from the reactor wall, and heat of calcination show that, for particles of effective spherical diameter of less than 10 μm (Biot number less than 0.1), the time for heating the particle from a temperature of 27°C to 1,000°C is less than 2 ms. As a result, the model assumes a flat temperature profile inside the particle during calcination and sulfation, and the energy balance is not incorporated in the comprehensive model development. The model also does not account for external heat transfer and mass transfer of SO_2 from the bulk gas phase to the surface of the particle.

Calcination and sintering

The calcination and sintering part of the combined model has been discussed by Ghosh-Dastidar et al. (1995) and applied for $Ca(OH)_2$ calcination kinetics and surface area development. The calcination takes place at the $CaCO_3/CaO$ interface and is assumed to be first order with respect to CO_2 partial pressure at the carbonate core surface (Silcox et al., 1989)

$$\gamma_s = k_c \frac{(P_e - P_c)}{RT} \tag{4}$$

From the solid reactant balance, the calcination rate can be expressed in terms of conversion as

$$\frac{dx_c}{dt} = \frac{3R_c^2 k_c (P_e - P_c)}{RTR_g^3 C_s} \tag{5}$$

where k_c (m/s) is the calcination rate constant and C_s (mol/m^3) is the solid reactant concentration. The equilibrium dissociation pressure P_e can be obtained as a function of temperature using a standard thermochemical approach (Hartman and Martinovsky, 1992).

The species continuity equation for product gas CO_2 diffusing through the product CaO assuming the pseudo-steady-state approximation can be written as

$$\frac{\partial^2 P}{\partial R^2} + \frac{2}{R}\frac{\partial P}{\partial R} = 0 \tag{6}$$

with the following boundary conditions

$$-D_{ce}\left.\frac{\partial P}{\partial R}\right|_{R=R_c} = k_c(P_e - P_c) \tag{7}$$

$$P|_{R=R_g} = 0 \tag{8}$$

The latter boundary condition assumes negligible bulk CO_2 concentration. Both Knudsen and ordinary diffusion may be important at different stages of the reaction and are considered in deriving the effective diffusivity. The effective diffusivity D_{ce} (m^2/s) is assumed to vary with structural parameters of the solids as per the model proposed by Wakao and Smith (1962).

Sintering is assumed to follow second-order kinetics as proposed by Nicholson (1965), and is experimentally verified for CaO particles by Silcox et al. (1989). The rate of surface area loss is given by

$$\frac{dS}{dt} = -k_{sm}(S - S_a)^2 \tag{9}$$

where S_a is the asymptotic surface area of CaO at the specific sintering temperature (m^2/g), and k_{sm} is the modified sintering rate constant ($g/m^2 \cdot s$).

The presence of CO_2 and H_2O is known to accelerate the rate of sintering of CaO (Borgwardt, 1985, 1989; Mai and Edgar, 1989). In order to account for enhanced sintering in the presence of CO_2, the sintering rate constant is modified according to the following correlation (Milne et al., 1990a):

$$k_{sm} = k_{\text{sin}}(1 + BP^m) \tag{10}$$

where k_{sin} is the sintering rate constant ($g/m^2 \cdot s$), and m and B are taken as 0.7 and 1.25, respectively, for $CaCO_3$ calcination (Milne et al., 1990a).

According to the model, the CaO shell is divided into multiple layers of subgrains depending on the time interval in which they are formed. The surface area of each subgrain layer is calculated by simultaneously solving Eqs. 5 through 10 numerically at each time step. At the end of the ith time interval, the CaO subgrain layer formed during the jth time interval will have a surface area ($S_{j,i}$) of

$$S_{j,i} = S_a + \frac{1}{[1/(S_o - S_a)] + \sum_{j=0}^{j} k_{sm_j}\Delta t} \tag{11}$$

where S_o (m^2/g) is the surface area of the nascent CaO formed at time t_j. In this study the value of S_o is assumed to be 107 m^2/g. The surface area of the entire product shell is calculated by summation over all the layers.

Relationship of sintering and porosity reduction is not clearly understood and the experimental data available in literature is rather ambiguous (Milne et al., 1990c). A host of previous studies have indicated a linear or logarithmic relationship between surface area and porosity in the low surface area-porosity range (Gullett and Bruce, 1987; Gullett and Blom, 1987; Milne et al., 1990c). In this work it is assumed that the porosity change $\Delta\epsilon$ is proportional to the change in CaO surface area ΔS, and porosity approaches zero as S approaches the asymptotic value S_a (Ghosh-Dastidar et al., 1995).

The calcination rate expression (Eq. 5) is coupled with the product CO_2 continuity equation (Eq. 6). The core radius R_c (m) is related to the solid conversion as

$$R_c = R_g(1 - x_c)^{1/3} \tag{12}$$

The instantaneous grain radius R_g (m) changes as a result of both calcination and sintering which work to oppose each other. Sintering alone causes the grains to grow by combination of adjacent grains. The model simulates the unreacted core of each small grain to remain at the center of the new grain and assumes that the grain size is not a function of the radial position inside the particle.

CaO-SO_2 reaction modeling

For irreversible reaction and diffusion of SO_2 in the calcined portion of the grain, assuming pseudo-steady-state condition, the mass balance for SO_2 can be written as

$$\frac{1}{R^2}\frac{\partial}{\partial R}\left(R^2 D_{se}\frac{\partial C_{SO_2}}{\partial R}\right) - r_{SO_2} = 0 \tag{13}$$

where

$$r_{SO_2} = \frac{3k_s}{r_g}(1 - \epsilon_s)C_{\text{ion}}C_{SO_2} \tag{14}$$

C_{ion} represents the concentration of ions at the reaction interface (mol/m^3). The local rate of reaction is assumed to be first-order with respect to SO_2 concentration and ion concentration on the surface of the subgrain. The boundary conditions are

$$C_{SO_2}|_{R=R_g} = C_{\text{bulk}} \tag{15}$$

$$\left.\frac{\partial C_{SO_2}}{\partial R}\right|_{R=R_c} = 0 \tag{16}$$

Both Knudson and molecular diffusivities are considered to calculate D_{se}, the effective diffusivity of SO_2. The local porosity following sulfation is given as

$$\epsilon_s = \epsilon - (z - 1)(1 - \epsilon)x_s \tag{17}$$

The reaction between SO_2 and Ca^{2+} in the presence of oxygen takes place at the surface of subgrains created as a result of calcination. Ca^{2+} and O^{2-} ions migrate in a coupled manner through the $CaSO_4$ layer to the surface. The pseudo-steady-state condition can be applied (Bischoff, 1963; Bowen, 1965; see Appendix) and the radial concentration profile of the ions in the $CaSO_4$ layer is given by

$$\frac{\partial}{\partial r}\left(r^2\frac{\partial C_{\text{ion}}}{\partial r}\right) = 0 \tag{18}$$

with the following boundary conditions

$$C_{\text{ion}}|_{r=r_c} = \rho_{\text{CaO}} \tag{19}$$

$$-D_{\text{ion}}\left(\frac{\partial C_{\text{ion}}}{\partial r}\right)\bigg|_{r=r_g} = k_s C_{\text{ion}} C_{\text{SO}_2} \tag{20}$$

where r_g and r_c represent the subgrain and the unreacted core radius, respectively.

The extent of sulfation for a given subgrain can be determined by performing a solid reactant balance

$$-\frac{dr_c}{dt} = \frac{k_s C_{\text{ion}} C_{\text{SO}_2} r_g^2}{\rho_{\text{CaO}} r_c^2} \tag{21}$$

The local conversion for a subgrain at a specific radial location inside the grain is given by

$$x_s = 1 - \left(\frac{r_c}{r_{\text{go}}}\right)^3 \tag{22}$$

The change in overall subgrain size is then obtained by taking into account the volume expansion due to sulfation

$$r_g^3 = r_c^3 + z x_s r_{\text{go}}^3 \tag{23}$$

The overall conversion for the entire grain is calculated by integrating the local conversion over all the layers of subgrains

$$X_s = \frac{3\int_{R_c}^{R_g} x_s R^2\, dR}{R_g^3} \tag{24}$$

In dimensionless form, Eqs. 13, 20, and 21 can be written as

$$\frac{1}{R^{*2}}\frac{\partial}{\partial R^*}\left[R^{*2} D_{se}^* \frac{\partial C_{\text{SO}_2}^*}{\partial R^*}\right] - \phi^2(1-\epsilon)\frac{C_{\text{ion}}^* C_{\text{SO}_2}^*}{r_g^*} = 0 \tag{25}$$

$$\frac{\partial C_{\text{ion}}^*}{\partial r^*}\bigg|_{r_g^*} = -\beta C_{\text{ion}}^* C_{\text{SO}_2}^* \tag{26}$$

$$\frac{\partial r_c^*}{\partial \tau} = -\frac{C_{\text{ion}}^* C_{\text{SO}_2}^* r_g^{*2}}{3 r_c^{*2}} \tag{27}$$

where

$$\phi = R_{\text{go}}\sqrt{\frac{3k_s\rho_{\text{CaO}}}{r_{\text{go}} D_{\text{bulk}}}} \tag{28}$$

represents a modified Thiele modulus and

$$\beta = \frac{k_s C_{\text{bulk}} r_{\text{go}}}{D_{\text{ion}}} \tag{29}$$

represents a modified Biot modulus, and τ is the dimensionless time.

The numerical simulation is carried out stepwise with time using the finite difference method. The calcination rate equation is coupled with the product CO_2 gas continuity equation; and the fourth-order Runge-Kutta integration is used to obtain both the calcination conversion and the product gas profile. The surface area and porosity of CaO layers formed at different times following sintering are used for sulfation calculations. The equations for SO_2 continuity and the solids conversion are coupled; and the implicit Crank-Nicolson technique is used to solve the initial value partial differential equations. The calcination is assumed to proceed unhindered by sulfation. At any given time t, the calcination has proceeded to a certain extent x_c and the overall sulfation to an extent X_s. There is a profile of SO_2 concentration, of calcium conversion, and of surface area and porosity. The combined model has four specific rate parameters k_c, k_{sin}, k_s, and D_{ion}, which are obtained from the best fit of experimental data and all of which follow an Arrhenius dependence with temperature.

Results and Discussion

Sulfation of MC: short-contact-time kinetics

The sulfation characteristics of MC are compared with two commercial sorbents under identical reaction conditions, a calcium carbonate (LC) and a calcium hydroxide (LH). The chemical composition and the initial surface area and pore properties of the sorbents are shown in Table 1. The primary particle-size distribution of the sorbents illustrates that the sorbents possess a unimodal distribution with the median particle diameter d_{50} between 1–3 μm for MC and LH and about 7 μm for LC. The *in-situ* particle sizing allows comparison of the different sorbents for the same particle size. As seen in Figure 3, the initial reaction rate of MC is more than two times that of LC, while its ultimate conversion is nearly 3 times that of the LC. The LC shows a virtual reaction die-off beyond 100 ms and its long-time conversion values of about 28% match with those reported by previous researchers (Milne et al., 1990c; Gullett et al., 1988). Mahuli et al. (1997)

Table 1. Chemical Composition and Initial Structural Properties of Sorbents

Composition (wt. %)	$Ca(OH)_2$* (LH)	$CaCO_3$* (LC)	Modified $CaCO_3$** (MC)
$Ca(OH)_2$	93.6	—	—
$CaCO_3$	1.0	97.0	97.0
SiO_2	0.8	0.8	0.8
Al_2O_3	0.6	0.5	0.6
MgO	1.0	—	1.0
CaO	1.0	—	—
Fe_2O_3	0.5	0.5	0.5
$MgCO_3$	—	1.0	—
BET Surface Area (m^2/g)	16.9	1.9	61.0
Pore Volume (cm^3/g)	0.06	0.004	0.121

*Linwood Mining and Minerals Co., Davenport, IA.
**Fan et al. (1998).

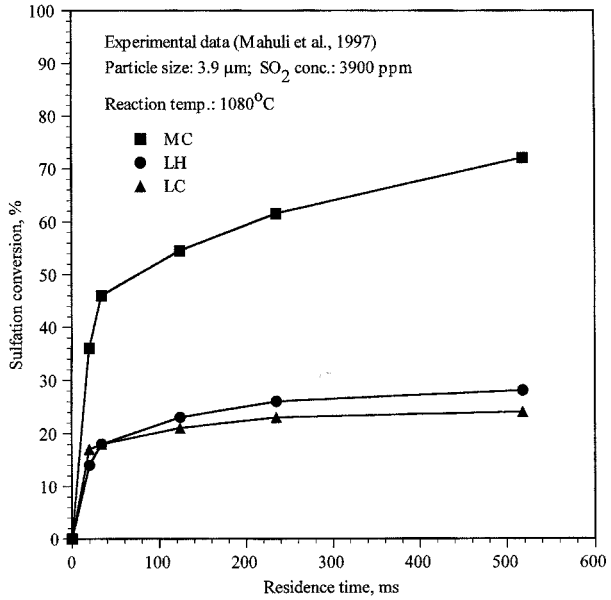

Figure 3. Short-contact-time sulfation data for MC, LH, and LC by Mahuli et al. (1997).

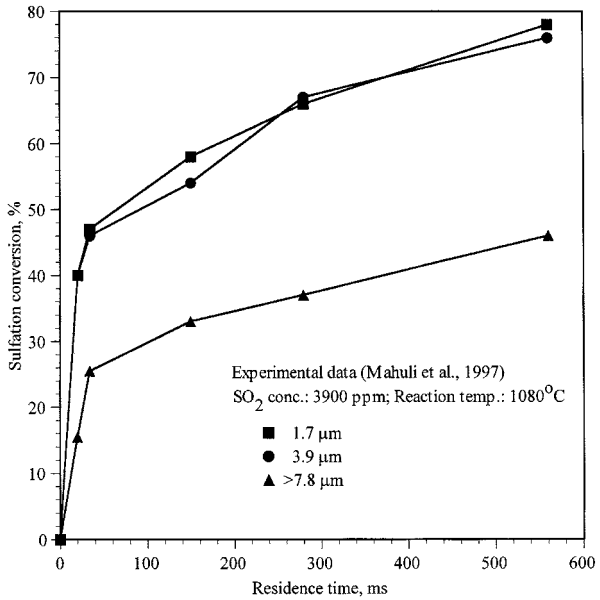

Figure 4. Effect of particle size on sulfation characteristics of MC by Mahuli et al. (1997).

have compared the MC with a high surface area hydroxide having similar particle size, surface area, and porosity. They have shown that the CaO from hydroxide sinters much faster than CaO from carbonate. In comparing LC and MC, Mahuli et al. (1997) have shown that even though CaO from LC possesses high surface area, its area is concentrated mainly in small pores < 50 Å in size. The CaO from MC has most of its surface area distributed in the 50–200 Å size range which is the primary reason for its exceptional reactivity.

In order to analyze the effects of intraparticle diffusional and heat-transfer limitations, sulfation conversions of various particle sizes at 1,000°C are shown in Figure 4. The 3.9 μm and 1.7 μm particles do not exhibit any difference in the initial rate or the longer-time conversion. Ghosh-Dastidar et al. (1995, 1996) showed that the LH also does not show significant particle-size effect below about 5 μm. This confirms similar observation made by previous investigators (Milne and Pershing, 1987).

Calcination and sintering modeling

The results of calcination modeling have been discussed by Ghosh-Dastidar et al. (1995) for LH. Here, the calcination results for MC are modeled and compared with LH. Figures 5 and 6 show the experimental data and model predictions for calcination of 3.9 μm MC and LH, respectively. The experimental data are obtained in the short-contact time EFR reactor under inert nitrogen conditions. The MC exhibits an extremely fast initial rate of calcination especially above 900°C and achieves more than 75% calcination, while conversion for LH progresses relatively slower at 900°C and tends to flatten beyond 50% at higher reaction times. For both the particles, most of the calcination is achieved within the first 50 ms at all the temperatures studied. The high initial surface area of MC contributes to its faster calcination kinetics and the model is able to predict that characteristic behavior.

The overall surface area evolution of the partially calcined MC shown in Figure 7 represents the net effect of two opposing phenomena of calcination and sintering. For comparison, the experimental data for LH and the model predictions (Ghosh-Dastidar et al., 1995) are shown in Figure 8. The surface area undergoes tremendous changes in the initial few milliseconds, and Figures 7 and 8 only show the net result of those changes. The surface area of nascent CaO has been measured at more than 100 m^2/g, however, the overall sur-

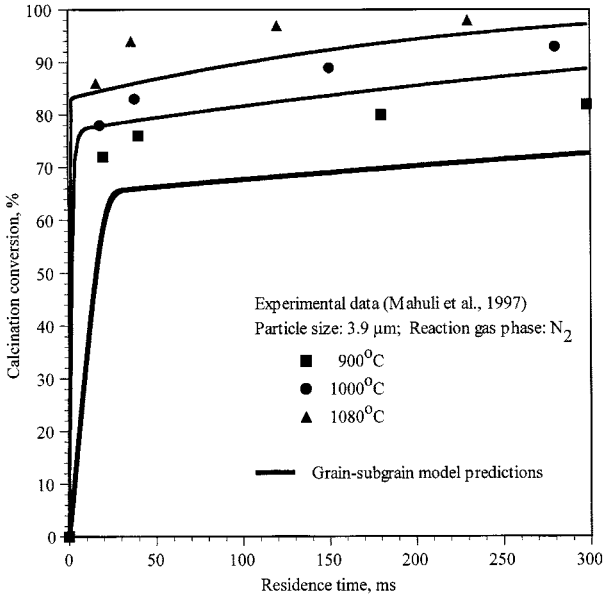

Figure 5. Predictions based on the grain-subgrain model for experimental data by Mahuli et al. (1997) for calcination kinetics of MC.

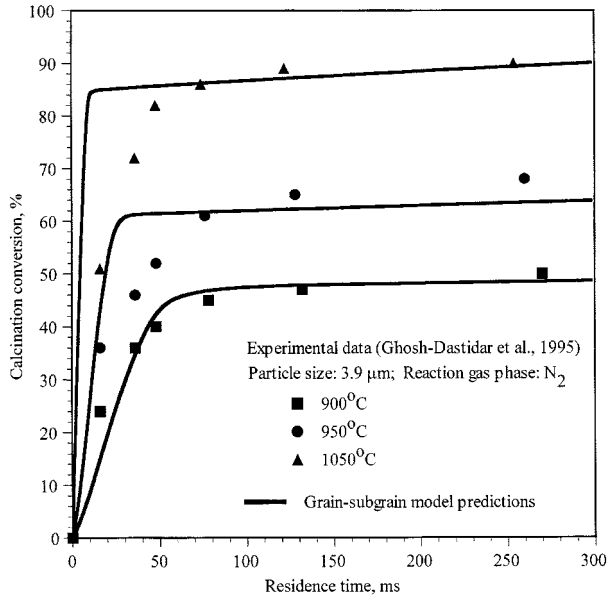

Figure 6. Predictions based on the grain-subgrain model for experimental data by Ghosh-Dastidar et al. (1995) for calcination kinetics of LH.

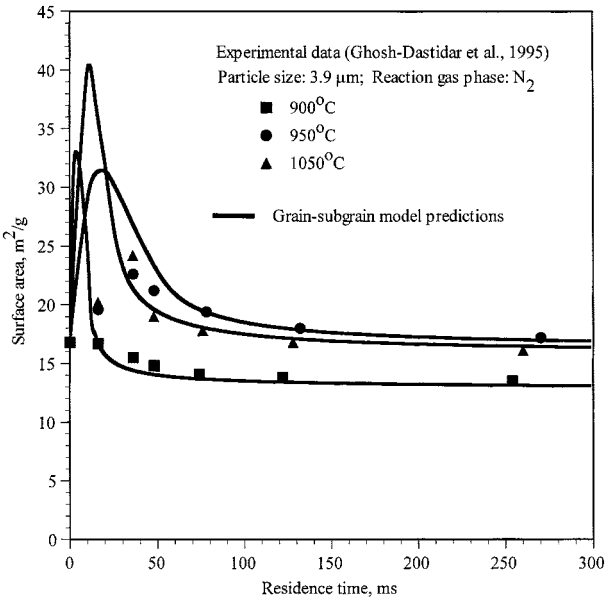

Figure 8. Predictions based on the grain-subgrain model for experimental data by Ghosh-Dastidar et al. (1995) for surface area evolution during calcination of LH.

face area never rises to those levels even after complete calcination. At 900°C, the calcination kinetics dominates over sintering; hence, the surface area initially rises above the parent, goes through a maximum, then rapidly decreases due to sintering and tends to level off to an asymptotic value at higher residence times. Another interesting point is that the higher the temperature, the earlier the maximum in surface area occurs. The grain-subgrain model incorporates the opposite competing influences of calcination and sintering on CaO surface area and predicts the maxima behavior, as well as the overall observed trends. The grain-subgrain model accounts for reduced surface area with fewer grains of larger diameter and vice versa. Figure 9 shows the model predictions of the grain and unreacted core size with calcination

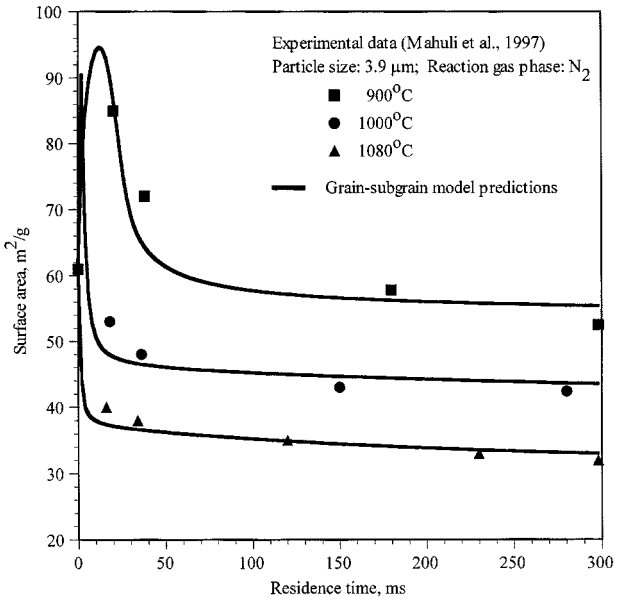

Figure 7. Predictions based on the grain-subgrain model for experimental data by Mahuli et al. (1997) for surface area evolution during calcination of MC.

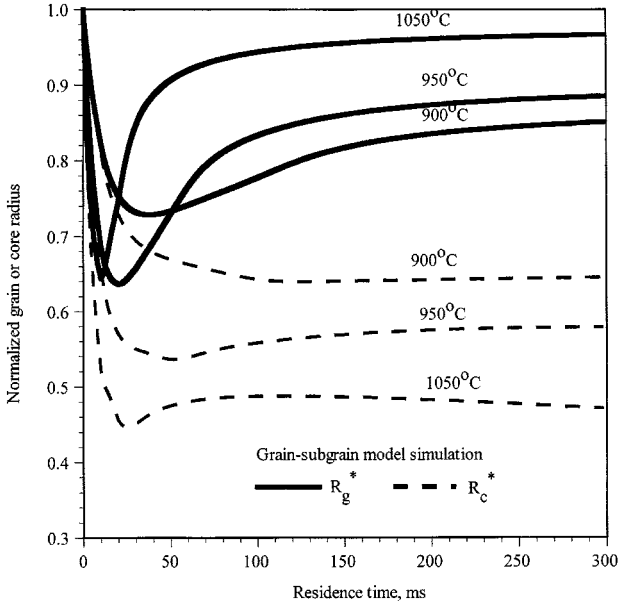

Figure 9. Grain-subgrain model simulation of the variation of the normalized grain and core radius with time during the calcination and sintering of LH.

and sintering. The grain size shown in Figure 9 for LH follows the opposite trend of surface area, initially decreasing to a minimum before increasing due to sintering.

The two rate parameters, the calcination rate constant k_c and the sintering rate constant k_{sin} are adjusted to obtain the best fit of the experimental data. The values of the rate constants and those reported in the literature are shown in Table 2. The sintering activation energies for MC and LH are quite similar and compare well with literature values which lie in the range of 50–65 kcal/mol. However, Borgwardt (1989) reported that the k_{sin} value for hydrate is an order of magnitude higher than for carbonate, while the k_{sin} values obtained from the grain-subgrain model are similar for LH and MC. It has been shown that the chemical composition and the level of impurities in the solid matrix have a significant influence on the sintering characteristics, which is probably the reason for the discrepancies in the k_{sin} values. Moreover, Borgwardt (1989) used a different model to analyze the surface area evolution behavior.

Table 2. Rate Parameters for Calcination and Sintering of MC and LH at 1,000°C from Grain-Subgrain Model

	MC	LH	Literature Values for $CaCO_3$ & $Ca(OH)_2$
k_c, m/s	0.9×10^{-3}	8×10^{-6}	5.4×10^{-3} for $CaCO_3$ (Silcox et al., 1989) 1.8×10^{-3} for $CaCO_3$ (Milne et al., 1990a)
k_{sin}, g/m^2·s	3.6×10^{-1}	2×10^{-1}	32×10^{-1} for $CaCO_3$ (Silcox et al., 1989)
E_c, kcal/mol	24.4	22.5	22 for carbonate; 16.4 for hydrate (Milne et al., 1990a)
E_{sin}, kcal/mol	59.8	57	~ 53 for both carbonate and hydrate (Borgwardt, 1989) ~ 59 for both carbonate and hydrate (Milne et al., 1990a) 77 for hydrate (Milne and Edgar, 1989)

CaO sulfation modeling

Equations 13 through 24 represent the model equations for the sulfation reaction alone and are solved numerically to investigate the sulfation model predictions and compare them with other models. In the absence of internal diffusional resistances ($\phi \ll 1$), chemical kinetics and product layer diffusion control the overall reaction rate and the conversion can be obtained in terms of the modified Biot modulus β for the grain-subgrain model. The corresponding equations for the random pore model and the spherical grain model (Bhatia and Perlmutter, 1981a) for $z = 1$, respectively are

$$x = 1 - \exp\left(\frac{1}{\psi} - \frac{\left[\sqrt{1+\beta\tau} - \left(1 - \frac{\beta}{\psi}\right)\right]^2 \psi}{\beta^2}\right) \tag{30}$$

$$\tau = 3\left[1-(1-x)^{1/3}\right] + \frac{3\beta}{4}\left[1-3(1-x)^{2/3}+2(1-x)\right] \tag{31}$$

Figure 10 compares the predictions of the grain-subgrain model with the random pore model and the grain model at two values of β. The agreement among the three different models is close, especially for the larger value of the modified Biot modulus β and for smaller conversions. The larger β represents increased product layer diffusional resistance, which, as expected, slows the progress of the conversion considerably.

In the presence of diffusional resistances, the porosity and surface area play an important role in determining the reaction rate and conversion behavior. Figure 11 shows the effect of initial porosity on the conversion characteristics when diffusional resistances dominate. The larger porosity significantly delays plugging and allows greater conversion. The conversion is also influenced by the surface area as well as by the dispersion of pore sizes. Bhatia (1985) and Christman and Edgar (1983) have shown that a less dispersed pore structure leads to increased maximum conversion. It has been postulated that the strong product layer diffusion resistance largely obscures the effect of pore-size distribution (Bhatia and Perlmutter, 1983). The grain-subgrain model does not incorporate the distribution of pore sizes (or grain sizes). Figure 12 indicates the effect of z, the molar volume ratio of product to reactant, on the conversion characteristics. At $z = 1$, a near complete conversion is attained since there are no porosity losses and diffusional resistances do not increase with reaction. At $z = 2$, the conversion is limited to only about 35%

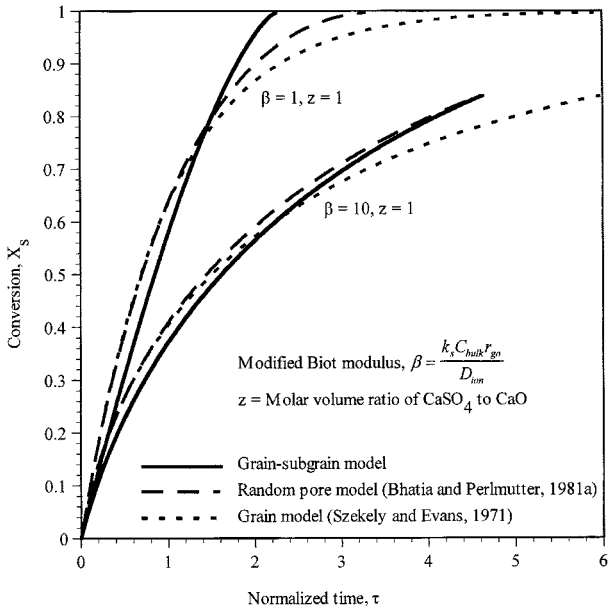

Figure 10. Conversion-time behavior predicted by grain-subgrain model, random pore model, and grain model at two values of modified Biot modulus when only effects of chemical reaction and product layer diffusion dominate.

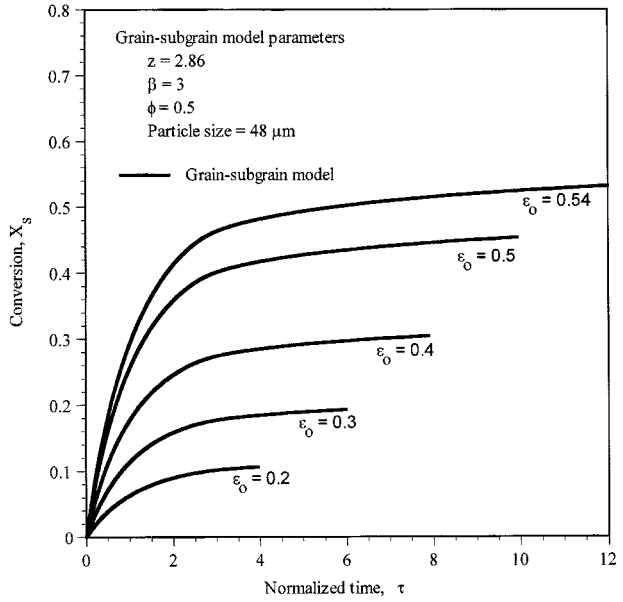

Figure 11. Grain-subgrain model predictions of the effect of CaO initial porosity on sulfation conversion.

for an initial porosity of 0.3. For CaO sulfation, the product $CaSO_4$ occupies nearly 3 times the volume of the reactant ($z = 2.86$) and with an initial porosity of 0.3, the theoretically predicted conversion is limited to less than 25%.

In order to demonstrate the application of the sulfation model, experimental CaO sulfation data reported in the literature are analyzed. The requirement for the sulfation data is that there should not be any concomitant sintering of CaO. Borgwardt (1970) represents one such study and the authors have obtained short-contact time sulfation data in the EFR reactor using precalcined and presintered CaO. The reaction parameters for Borgwardt's (1970) data in the temperature range of 650 to 980°C are listed in Table 3. Figure 13 shows the computed results obtained from the grain-subgrain model superimposed on the experimental data of Borgwardt (1970). The two rate parameters k_s and D_{ion} represent the only fitting parameters. k_s can be obtained from initial rate data leaving D_{ion} (or β) as the only adjustable parameter. The best fit values of k_s and D_{ion} are listed in Table 4 along with the values reported by Bhatia and Perlmutter (1981b). The random pore model predictions of the same data are presented in Figure 14. The random pore model predicts a stop in the reaction at the stage of surface pore plugging. The grain-subgrain model uses the residual porosity concept first introduced by Hartman and Coughlin (1976) based on their experimental observations. The residual porosity value of 0.005 used in these computations is based on Hartman and Coughlin (1976). The value $k_s = 6.0 \times 10^{-5}$ m^4/kmol·s obtained from the grain-subgrain model at 870°C compares well with the value $k_s = 4.7 \times 10^{-5}$ m^4/kmol·s for the random

Table 3. Experimental Parameter Values Applied to the CaO Sulfation Data of Borgwardt (1970)

Experimental Parameter	Numerical Value
ϵ_o	0.56
R_{go}	48 μm
S_o	5.9×10^6 m^2/m^3
C_{bulk}	3,000 ppmv
ρ_{CaO}	3.32 g/cm^3

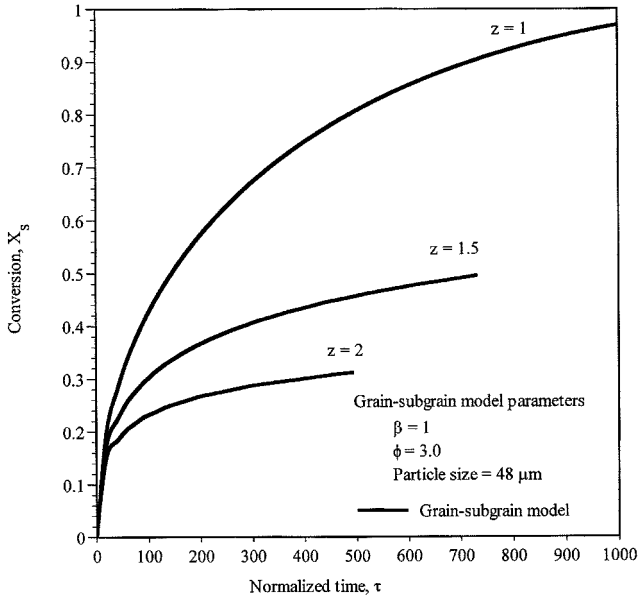

Figure 12. Grain-subgrain model predictions of the effect of z, the molar volume ratio of $CaSO_4$ to CaO, on sulfation conversion of CaO.

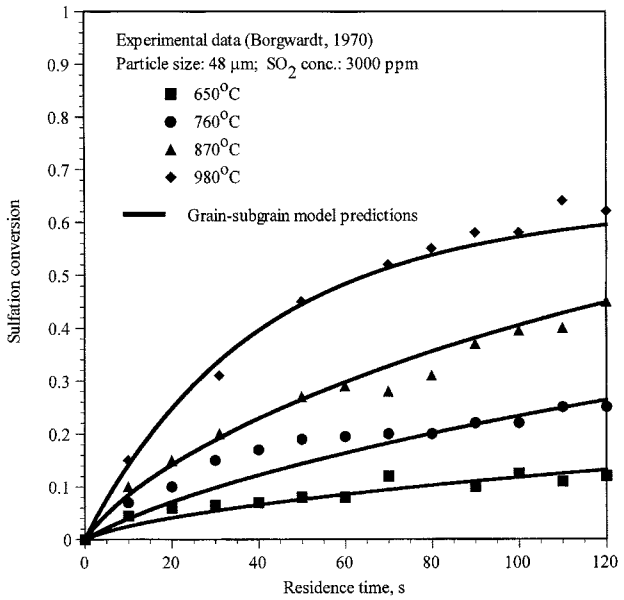

Figure 13. Predictions based on the grain-subgrain model for experimental data on sulfation of CaO by Borgwardt (1970).

Table 4. Model Parameters from Grain-Subgrain Model vs. Random Pore Model*

	Grain-Subgrain Model	Random Pore Model (Bhatia and Perlmutter, 1981b)
k_s, m^4/mol·s	3.8×10^{-8}	8.34×10^{-8}
D_{ion}, m^2/s	2.1×10^{-16}	69×10^{-12}
β	0.1	6.3
E_s, kcal/mol	14.7	13.4
E_{ion}, kcal/mol	27.9	30

*The experimental data are the CaO sulfation kinetics from Borgwardt (1970) at 980°C.

pore model. In the literature, the value of the sulfation rate constant varies considerably. For example, Hartman and Coughlin (1976) obtained a higher value $k_s = 111.5\times10^{-5}$ m^4/kmol·s at 850°C by using the grain model to fit their data, while Ramachandran and Smith (1977) calculated $k_s = 1.7\times10^{-5}$ m^4/kmol·s at the same temperature. The sulfation and PLD activation energies obtained from the grain-subgrain model are 14.7 and 27.9 kcal/mol respectively, compared to 13.4 and 30 kcal/mol estimated by Bhatia and Perlmutter (1981b).

The product layer diffusivity is very difficult to measure experimentally and its value is generally obtained from fitting the experimental data to an appropriate model (Berniere and Catlow, 1983). As a result, its value depends on the particular mechanistic model used. The ionic diffusion in solids could occur by various mechanisms such as interstitial or vacancy. For a true crystal (without defects or vacancies), the final equation for diffusivity can be expressed as (Shewmon, 1989),

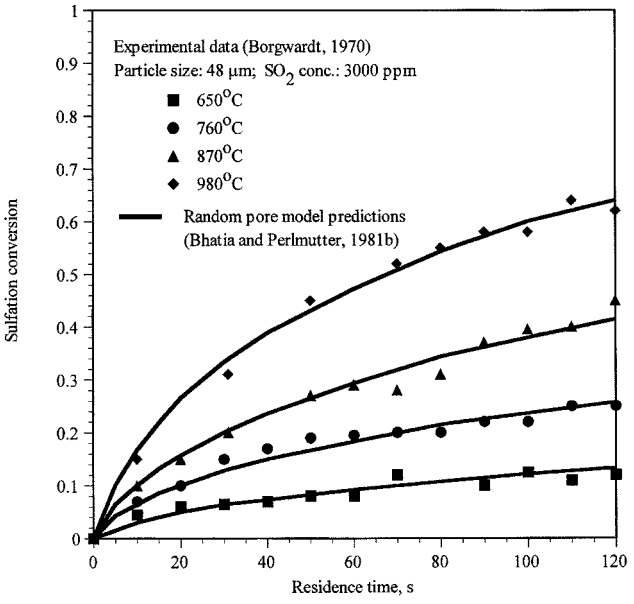

Figure 14. Predictions based on the random pore model of Bhatia and Perlmutter (1981b) for the experimental data on sulfation of CaO by Borgwardt (1970).

Adapted from Bhatia and Perlmutter, 1981b.

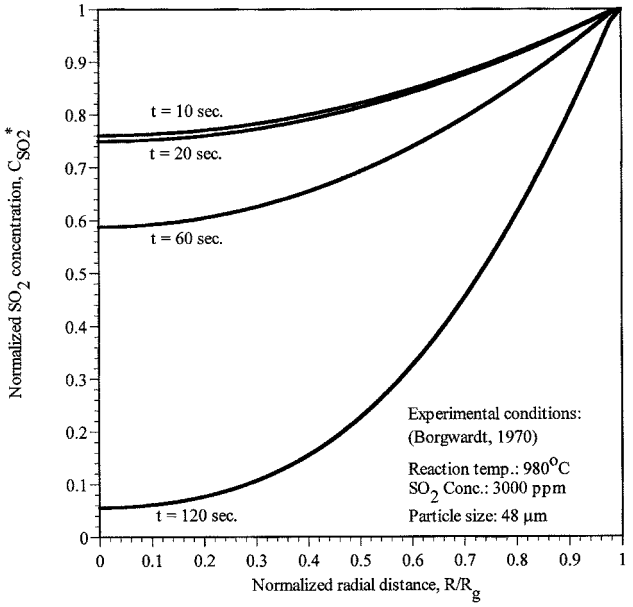

Figure 15. Simulated variation in the SO_2 concentration profile with time and radial distance based on the grain-subgrain model for the experimental conditions of Borgwardt (1970).

$$D = D_o \exp\left(\frac{-\Delta H_f - \Delta H_m}{RT}\right) \qquad (32)$$

ΔH_f is the energy of vacancy formation and ΔH_m is the energy of vacancy migration per vacancy. In the case of $CaSO_4$ structure doped with CaO, defects already exist due to impurities; and thus only ΔH_m can be considered. An estimate of the magnitude of diffusivity of Ca^{2+} ions through the $CaSO_4$ can be obtained from estimates of D_o and ΔH_m. Typically, D_o depends on the size of the diffusing ions and has values in the range of 10^{-3} cm^2/s. For ΔH_m, an average value of about 2.5 eV is an acceptable estimate for the energy of vacancy migration (Shewmon, 1989). The estimated value for diffusivity of Ca^{2+} ions is about 10^{-15} m^2/s based on the above values. The value of D_{ion} obtained from the grain-subgrain model is in the range of 10^{-15}–10^{-17} m^2/s.

Figures 15 and 16 show the predicted radial concentration profile for SO_2 and the local subgrain conversion profile inside the grain at various times. The SO_2 concentration decreases continuously with time as a result of consumption as well as increasing diffusional resistance. The profile of ionic concentration at the surface of the subgrain is shown in Figure 17 for three locations in the grain. Before the buildup of the product layer, the ionic concentration is the same everywhere as the solid CaO concentration. As the reaction proceeds, the product layer offers increased resistance to ionic diffusion. In addition, the local SO_2 concentration also influences the ionic concentration profile. In the initial stages of SO_2 exposure, the porosity reduction due to sulfation is not drastic and a significant amount of SO_2 can diffuse inside and react with the surface ions thus lowering their concentra-

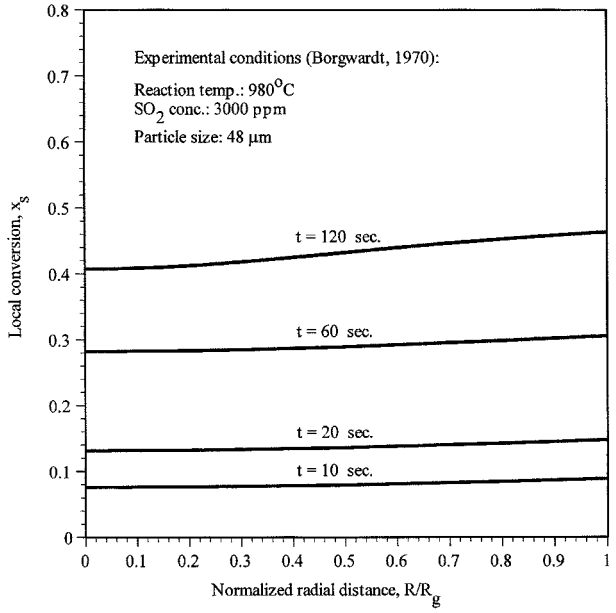

Figure 16. Simulated variation in the local conversion with time and radial distance based on the grain-subgrain model for the experimental conditions of Borgwardt (1970).

tion. As the reaction proceeds, the SO_2 concentration especially in the interior of the grain reduces significantly and, subsequently, the ion concentration in the interior of the grain ($R = R_c$) increases.

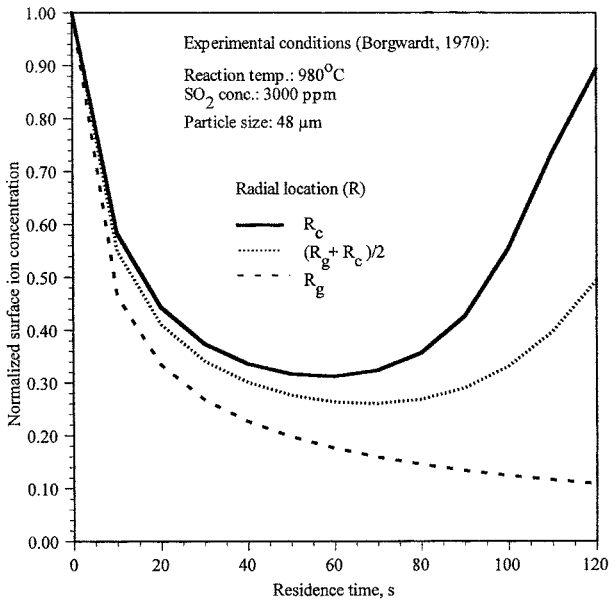

Figure 17. Simulated variation of the subgrain surface ion concentration with time at three radial positions based on the grain-subgrain model for the experimental conditions of Borgwardt (1970).

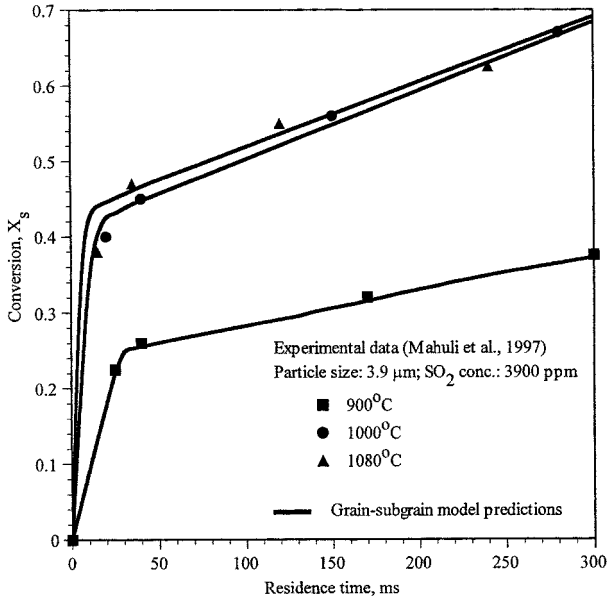

Figure 18. Predictions based on the grain-subgrain model for experimental data by Mahuli et al. (1997) for the sulfation kinetics of MC.

Combined calcination, sintering and sulfation modeling

The application of the combined model is demonstrated for short-contact time sulfation data of MC and LH. Figure 18 shows the results for the simultaneous calcination, sintering, and sulfation of 3.9 μm MC particles. Initially, sulfation progresses extremely fast reaching nearly 50% conversion in less than 50 milliseconds. Moreover, the initial sulfation rate is very similar for 1,000°C and 1,080°C, with the higher reaction time data indicating slightly higher conversion at 1,000°C than at 1,080°C. This is indicative of an optimum sulfation temperature for MC. Mahuli et al. (1997) investigated sulfation at various temperatures between 900°C and 1,100°C and showed that 1,020°C exhibits the highest sulfation conversion at longer reaction times. A number of previous researchers have observed this phenomenon of optimum temperature for $CaCO_3$ sulfation; however, the estimates of optimum have varied widely between 1,000 to 1,150°C. Milne et al. (1990c) predicted the optimum temperature to be 1,065°C using their model, while Alvfors and Svedberg (1992) reported it to be 1,027°C from their PSS model. Bortz and Flament (1985) experimentally observed the optimum to be 1,090°C, while Wang et al. (1995) reported a temperature of 1,050°C. This phenomenon during combined calcination, sintering and sulfation of $CaCO_3$ can be explained as follows. As the temperature increases, the rate of reaction and product layer diffusion increase. However, the rate of sintering is also considerably enhanced with increasing temperature (due to its high activation energy of > 50 kcal/mol). This leads to a greater loss of porosity which hinders the transport of SO_2 into the interior. Furthermore, the $CaSO_4$ vapor pressure may also begin to exert an influence on the overall reaction and lead to decomposition of the product at higher temperatures (Milne et al., 1990c). These opposing effects together lead to an optimum temperature for sulfation. The grain-subgrain model closely predicts the initial steep slope and the rate at-

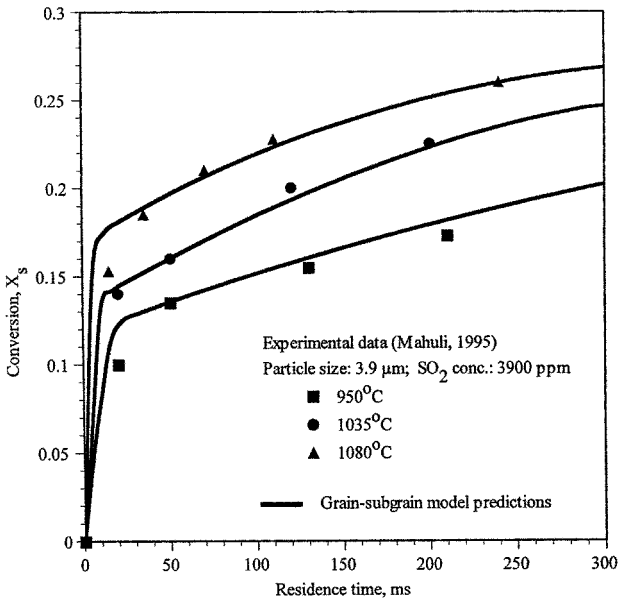

Figure 19. Predictions based on the grain-subgrain model for experimental data by Mahuli (1995) for the sulfation kinetics of LH.

tenuation characteristics. However, for the reaction temperature of 1,080°C, the model overestimates the initial rate; but at higher residence times, its predictions match well with the experimental data.

Figure 19 shows the experimental data and grain-subgrain model predictions for simultaneous calcination and sulfation of LH. For the three temperatures shown in the figure, the rate of reaction and the final conversion continuously increase with temperature, and an optimum temperature is not clearly obvious from the data. Investigations to precisely ascertain the optimum temperature were not conducted as part of this study. Milne et al. (1990c) have reported an optimum of about 1,120°C.

Table 5 shows the values of the adjustable rate parameters obtained from fitting the grain-subgrain model for MC and LH sulfation. The inputs to the model include the initial pore properties of MC and LH listed in Table 1, the SO_2 bulk concentration (3,900 ppmv), and the particle size (3.9 μm). The k_c and k_{sin} are fixed at the values obtained from the calcination and sintering model (Table 2) and are not varied in modeling the combined data in Figures 18 and 19. The k_s and D_{ion} values in Table 4 obtained from fitting the grain-subgrain model to Borgwardt's (1970) data are used as initial guesses. The sulfation rate constant k_s is found to be nearly

Table 5. Model Parameters for LH and MC Sulfation at 1,080°C Obtained by Fitting Grain-Subgrain Model to the Short-Contact-Time Data

Model Parameters	MC	LH
k_s, $m^4/mol \cdot s$	1.6×10^{-5}	2.3×10^{-5}
D_{ion}, m^2/s	4.0×10^{-17}	3.0×10^{-16}
E_s, kcal/mol	18.2	14.5
E_{ion}, kcal/mol	26	32.6

three orders of magnitude higher for short-contact time MC and LH sulfation data. The value for k_s obtained for experimental data (Borgwardt, 1970) using the grain-subgrain model is at a sulfation reaction temperature of 980°C for 45 μm CaO particles following reaction for 100–150 s. Because of large particle size and lower reaction temperatures, it is plausible that the kinetic data obtained by Borgwardt (1970) suffers from external transport limitations. This would result in lower conversions for these particles than the smaller particles (MC and LH) after similar exposure times. The grain-subgrain model is developed without considering the external transport limitations and, since k_s is an adjustable parameter for the grain-subgrain model, a lower value of k_s is obtained for large particles where external transport limitations dominate the overall sulfation process.

Conclusions

The grain-subgrain model presented in this study incorporates three simultaneously occurring phenomena when a $CaCO_3$ or $Ca(OH)_2$ sorbent particle interacts with SO_2 in the high-temperature environment of a fossil fuel combustor. This model includes for the first time the solid-state diffusion parameters of the ionic species in the product layer, which is the fundamental limiting factor on reaction rate and total conversion. The calcination is described by first-order kinetics, and the resulting CaO formed from $CaCO_3$/$Ca(OH)_2$ grains is visualized as being composed of layers of subgrains. The sintering is described as a second-order process with subgrain layers having different surface area and porosities due to different extents of sintering. The calcination and sintering are together used to predict the local surface area and porosity as functions of time, which are used in calculating the local sulfation of the individual subgrains. The grain-subgrain model incorporates the solid-state ionic diffusion of Ca^{2+} and O^{2-} in a coupled manner through the product phase to the outer surface of the subgrain where it reacts with SO_2. The model matches the experimental data from a differential fixed-bed reactor with an SO_2 exposure time of a few seconds, as well as ultrafast short-contact-time data from an isothermal high-temperature entrained flow reactor at SO_2 exposure times of under 500 ms. The proposed model can be used to predict independent calcination, CaO sulfation, as well as combined calcination, sintering, and sulfation data for $CaCO_3$ and $Ca(OH)_2$. The predictions of the proposed model are compared with those of the random pore model and the grain model. The values of k_c and k_{sin} compare well with those previously reported. The product layer diffusion coefficient has shown considerable variation in the literature and its value is known to depend on the choice of the model. The grain-subgrain model with its coupled diffusion of Ca^{2+} and O^{2-} ions through the $CaSO_4$ matrix gives a product layer diffusivity of the order of 10^{-16} m^2/s while the previously reported values lie in the range of 10^{-12}–10^{-14} m^2/s. The sulfation and PLD activation energies obtained from the grain-subgrain model are 14.7 and 27.9 kcal/mol, respectively, and compare well with the reported values.

Acknowledgments

This work was supported in part by the Ohio Coal Development Office. The authors would like to thank Dr. A. Ghosh-Dastidar for

his insightful comments and suggestions, and Mr. Himanshu Gupta for his help with the analyses.

Notation

C_{ion} = concentration of calcium ions at the surface of the subgrain, mol/m^3
$C^*_{ion} = C_{ion}/\rho_{CaO}$, dimensionless ionic concentration
C_{bulk} = concentration of SO_2 in the bulk gas phase, mol/m^3
C_{SO_2} = concentration of SO_2 inside the grain, mol/m^3
$C^*_{SO_2} = C_{SO_2}/C_{bulk}$, dimensionless SO_2 concentration
D = diffusivity in Eq. 32
D_o = pre-exponential factor in Eq. 32
D_{se} = effective diffusivity of SO_2 through the grain, m^2/s
D_{bulk} = bulk diffusivity of SO_2, m^2/s
$D^*_{se} = D_{se}/D_{bulk}$, dimensionless SO_2 diffusivity
D_{ion} = ionic diffusivity, m^2/s
E_c = activation energy for calcination reaction, kcal/mol
E_{sin} = activation energy for sintering, kcal/mol
E_s = activation energy for sulfation reaction, kcal/mol
k_s = specific rate constant for CaO sulfation, m^4/mol·s
P = partial pressure of CO_2 in the CaO product layer
P_c = partial pressure of CO_2 at the CaO/$CaCO_3$ interface
r = distance along subgrain, m
r_c = unreacted core radius of CaO subgrain, m
r_g = subgrain radius, m
r_{go} = initial subgrain radius, m
$r^* = r/r_{go}$, dimensionless subgrain radius
R = radial distance in the grain, m
R = universal gas constant in Eqs. 4, 5, and 32
R_{go} = initial grain radius, m
$R^* = R/R_{go}$, dimensionless grain radius
S = specific surface area of CaO, m^2/g
S_o = specific surface area of nascent CaO, m^2/g
$S_{j,i}$ = specific surface area of CaO formed at time t_j at the end of time t_i, m^2/g
T = temperature, K
x_c = extent of calcination of $CaCO_3$
x_s = local extent of sulfation
X_s = overall conversion of $CaCO_3$ to $CaSO_4$
z = molar volume ratio of $CaSO_4$ to CaO

Greek letters

β = modified Biot modulus
ΔH_f = energy of vacancy formation per vacancy
ΔH_m = energy of vacancy migration per vacancy
Δt = time increment, seconds
ϵ_s = local product layer porosity following sulfation
ϵ_o = initial porosity of CaO
ϵ = local porosity of CaO at any time t following sintering
γ_s = rate of $CaCO_3$ calcination reaction, mol/m^2·s
λ = perturbation parameter given in Eq. A6
ϕ = modified Thiele modulus
ψ = structural parameter used in random pore model
ρ_{CaO} = density of CaO, mol/m^3
$\tau = 3k_sC_{bulk}t/r_{go}$, dimensionless time

Literature Cited

Alvfors, P., and G. Svedberg, "Modeling of the Sulfation of Calcined Limestone and Dolomite—A Gas-Solid Reaction with Structural Changes in the Presence of Solids," *Chem. Eng. Sci.*, **43**, 1183 (1988).

Alvfors, P., and G. Svedberg, "Modelling of the Simultaneous Calcination, Sintering and Sulfation of Limestone and Dolomite," *Chem. Eng. Sci.*, **47**(8), 1903 (1992).

Berniere, F., and C. R. A. Catlow, *Mass Transport in Solids*, Plenum, NY (1983).

Bhatia, S. K., and D. D. Perlmutter, "A Random Pore Model for Fluid-Solid Reactions: I. Isothermal, Kinetic Control," *AIChE J.*, **26**(3), 379 (1980).

Bhatia, S. K., and D. D. Perlmutter, "A Random Pore Model for Fluid-Solid Reactions: II. Diffusion and Transport Effects," *AIChE J.*, **27**(2), 247 (1981a).

Bhatia, S. K., and D. D. Perlmutter, "The Effect of Pore Structure on Fluid-Solid Reactions: Application to the SO_2-Lime Reaction," *AIChE J.*, **27**(2), 226 (1981b).

Bhatia, S. K., and D. D. Perlmutter, "Effect of Product Layer on the Kinetics of the CO_2-Lime Reaction," *AIChE J.*, **29**(1), 79 (1983).

Bhatia, S. K., "Analysis of Distributed Pore Closure in Gas-Solid Reactions," *AIChE J.*, **31**(4), 642 (1985).

Bischoff, K. B., "Accuracy of the Pseudo-Steady State Approximation for Moving Boundary Diffusion Problems," *Chem. Eng. Sci.*, **18**, 711 (1963).

Borgwardt, R. H., "Kinetics of Reaction Between SO_2 and Calcined Limestone," *Environ. Sci. Technol.*, **4**, 59 (1970).

Borgwardt, R. H., K. R. Bruce, and J. Blake, "An Investigation of Product-Layer Diffusivity for CaO Sulfation," *Ind. Eng. Chem. Res.*, **26**, 1993 (1987).

Borgwardt, R. H., "Sintering of Nascent Calcium Oxide," *Chem. Eng. Sci.*, **44**(1), 53 (1989).

Borgwardt, R. H., "Calcination Kinetics and Surface Area of Dispersed Limestone Particles," *AIChE J.*, **31**, 103 (1985).

Borgwardt, R. H., and K. R. Bruce, "Effect of Specific Surface Area on the Reactivity of CaO with SO_2," *AIChE J.*, **32**(2), 239 (1986).

Bortz, S. J., and P. Flament, *Recent IFRF Fundamental and Pilot Scale Studies on the Direct Sorbent Injection Process, Proc.: First Joint Symp. on Dry SO_2 and Simultaneous SO_2/NO_x Control Technologies*, 1, EPA-600/9-85/020a, (NTIS PB85-232353) (1985).

Bowen, J. R., "Comments on the Pseudo-Steady State Approximation for Moving Boundary Problems," *Chem. Eng. Sci.*, **20**, 712 (1965).

Bruce, K. R, B. K. Gullet, and L. O. Beach, "Comparative SO_2 Reactivity of CaO Derived from $CaCO_3$ and $Ca(OH)_2$," *AIChE J.*, **35**, 37 (1989).

Calvelo, A., and J. M. Smith, "Intrapellet Transport in Gas Solid Noncatalytic Reactions," *Proc. of Chemeca 70*, Butterworths, Australia (1971).

Christman, P. G., and T. F. Edgar, "Distributed Pore-Size Model for Sulfation of Limestone," *AIChE J.*, **29** (1983).

Duo, W., J. P. K. Sevill, N. F. Kirkby, and R. Clift, "Formation of Product Layers in Solid-Gas Reactions for Removal of Acid Gases," *Chem. Eng. Sci.*, **49**, 4429 (1994).

Evans, R. C., *An Introduction to Crystal Chemistry*, 2nd ed., Cambridge Univ. Press, Cambridge (1964).

Fan, L.-S., S. Satija, W. I. Wilson, D. C. Fee, K. M. Myles, and I. Johnson, "Thermogravimetric Analysis of Sulfation Kinetics of Calcined Limestones or Dolomites," *Chem. Eng. J.*, **28**, 151 (1984).

Fan, L.-S., A. Ghosh-Dastidar, and S. K. Mahuli, "Chemical Sorbent and Methods of Making and Using Same," U.S. Patent No. 08/584,089 (Jan. 6, 1998).

Georgakis, C., C. W. Chang, and J. Szekely, "A Changing Grain Size Model for Gas-Solid Reactions," *Chem. Eng. Sci.*, **34**, 1072 (1979).

German, R. M., and Z. A. Munir, "Surface Area Reduction During Isothermal Sintering," *J. Amer. Ceram. Soc.*, **59**, 379 (1976).

Ghosh-Dastidar, A., S. Mahuli, R. Agnihotri, and L.-S. Fan, "Ultrafast Calcination and Sintering of $Ca(OH)_2$ Powder: Experimental and Modeling," *Chem. Eng. Sci.*, **50**, 2029 (1995).

Ghosh-Dastidar, A., S. Mahuli, R. Agnihotri, and L.-S. Fan, "Investigation of High-Reactivity Calcium Carbonate Sorbent for Enhanced SO_2 Capture," *Ind. Eng. Chem. Res.*, **35**, 598 (1996).

Gullett, B. K., and J. A. Blom, "Calcium Hydroxide and Calcium Carbonate Particle Size Effects on Reactivity with Sulfur Dioxide," *Reactivity of Solids*, **3**, 337 (1987).

Gullett, B. K., and K. R. Bruce, "Pore Distribution Changes of Calcium Based Sorbents Reacting with Sulfur Dioxide," *AIChE J.*, **33**, 1719 (1987).

Gullett, B. K., J. A. Blom, and G. R. Gillis, "Design and Characterization of a 1,200°C Entrained Flow, Gas/Solid Reactor," *Rev. Sci. Instrum.*, **59**, 1980 (1988).

Hartman, M., and R. W. Coughlin, "Reaction of Sulfur Dioxide with Limestone and the Grain Model," *AIChE J.*, **22**, 490 (1976).

Hartman, M., and A. Martinovsky, "Thermal Stability of the Magnesium and Calcareous Compounds for Desulfurization Processes," *Chem. Eng. Commun.*, **111**, 149 (1992).

Hsia, C., G. R. St. Pierre, K. Raghunathan, and L.-S. Fan, "Diffusion through $CaSO_4$ Formed during the Reaction of CaO with SO_2 and O_2," *AIChE J.*, **39**, 698 (1993).

Hsia, C., G. R. St. Pierre, and L.-S. Fan, "Isotope Study on Diffusion in $CaSO_4$ Formed during Sorbent Flue Gas Reaction," *AIChE J.*, **41**, 2337 (1995).
Kirchgessner, D. A., and W. Jozewicz, "Enhancement of Reactivity in Surfactant-Modified Sorbents for Sulfur Dioxide Control," *Ind. Eng. Chem. Res.*, **28**, 413 (1989).
Li, X., Z. Luo, M. Ni, and K. Cen, "Modeling Sulfur Retention in Circulating Fluidized Bed Combustors," *Chem. Eng. Sci.*, **50**, 2235 (1995).
Lindner, B., and D. Simonsson, "Comparison of Structural Models for Gas-Solid Reactions in Porous Solids Undergoing Structural Changes," *Chem. Eng. Sci.*, **36**, 1519 (1981).
Mahuli, S. K., "Mechanistic Studies of Ultrafast SO_2 and Selenium Removal by Calcium-Based Sorbents," PhD Diss., The Ohio State Univ., Columbus (1995).
Mahuli, S. K., R. Agnihotri, S. Chauk, A. Ghosh-Dastidar, S.-H. Wei, and L.-S. Fan, "Pore Structure Optimization of Calcium Carbonate for Enhanced Sulfation," *AIChE J.*, **43**, 2323 (1997).
Mai, M. C., and T. F. Edgar, "Surface Area Evolution of Calcium Hydroxide during Calcination and Sintering," *AIChE J.*, **35**, 30 (1989).
Milne, C. R., and D. W. Pershing, "Time Resolved Sulfation Rate Measurements for Sized Sorbents," *Proc. Pittsburgh Coal Conf.*, 109 (1987).
Milne, C. R., and D. W. Pershing, "An Experimental and Theoretical Study of the Fundamentals of the SO_2/Lime Reaction at High Temperatures," presented at the First Combined FGD and Dry SO_2 Control Symposium, EPA/EPRI, St. Louis, MO (Oct. 25–28, 1988).
Milne, C. R., G. R. Silcox, D. W. Pershing, and D. A. Kirchgessner, "Calcination and Sintering Models for Application to High-Temperature, Short-Time Sulfation of Calcium-Based Sorbent," *Ind. Eng. Chem. Res.*, **29**, 139 (1990a).
Milne, C. R., G. R. Silcox, D. W. Pershing, and D. A. Kirchgessner, "High-Temperature, Short-Time Sulfation of Calcium-Based Sorbents. 1. Theoretical Sulfation Model," *Ind. Eng. Chem. Res.*, **29**(11), 2192 (1990b).
Milne, C. R., G. R. Silcox, D. W. Pershing, and D. A. Kirchgessner, "High-Temperature, Short-Time Sulfation of Calcium-Based Sorbents. 2. Experimental Data and Theoretical Model Predictions," *Ind. Eng. Chem. Res.*, **29**(11), 2201 (1990c).
Nicholson, D., "Variation of Surface Area during the Decomposition of Solids," *Trans. Farad. Soc.*, **61**, 990 (1965).
Pigford, R. L., and L. Sliger, "Rate of a Diffusion Controlled Reaction Between a Gas and a Porous Solid Sphere," *Ind. Eng. Chem. Proc. Des. & Dev.*, **12**, 85 (1973).
Raghunathan K., A. Ghosh-Dastidar, and L.-S. Fan, "A Technique for the Study of Ultrafast Gas-Solid Reactions for Residence Times less than 100 ms," *Rev. Sci. Instrum.*, **63**, 5469 (1992).
Raghunathan, K., A. Ghosh-Dastidar, and L.-S. Fan, "High Temperature Reactor System for Study of Ultrafast Gas-Solid Reactions," *Rev. Sci. Instrum.*, **64**, 1989 (1993).
Ramachandran, P. A., and J. M. Smith, "Effect of Sintering and Porosity Changes on the Rate of Gas-Solid Reactions," *Chem. Eng. J.*, **14**, 137 (1977).
Ramachandran, P. A., and L. K. Doraiswamy, "Modeling of Non-Catalytic Gas-Solid Reactions," *AIChE J.*, **28**(6), 881 (1982).
Ranade, P. V., and D. P. Harrison, "The Grain Model Applied to Porous Solids with Varying Structural Properties," *Chem. Eng. Sci.*, **34**, 427 (1979).
Ranade, P. V., and D. P. Harrison, "The Variable Property Grain Model applied to the Zinc Oxide-Hydrogen Sulfide Reaction," *Chem. Eng. Sci.*, **36**, 1079 (1981).
Reyes, S., and K. F. Jensen, "Percolation Concepts in Modeling of Gas-Solid Reactions: III. Application to Sulfation of Calcined Limestone," *Chem. Eng. Sci.*, **42**, 565 (1987).
Sadakata, M., T. Shinbo, A. Harano, H. Yamamoto, and H. J. Kim, "Removal of SO_2 from Flue Gas Using Ultrafine CaO Particles," *J. Chem. Eng. of Japan*, **27**, 550 (1994).
Shewmon, P. G., *Diffusion in Solids*, McGraw-Hill, New York (1989).
Silcox, G. D., J. C. Kramlich, and D. W. Pershing, "A Mathematical Model for the Flash Calcination of Dispersed $CaCO_3$ and $Ca(OH)_2$ Particles," *Ind. Eng. Chem. Res.*, **28**, 155 (1989).
Simons, G. A., and A. R. Garman, "Small Pore Closure and the Deactivation of the Limestone Sulfation Reaction," *AIChE J.*, **32**, 1491 (1986).
Simons, G. A., A. R. Garman, and A. A. Boni, "The Kinetic Rate of SO_2 Sorption by CaO," *AIChE J.*, **33**, 211 (1987).
Sotirchos, S. V., "On a Class of Random Pore and Grain Models for Gas-Solid Reactions," *Chem. Eng. Sci.*, **42**, 1262 (1987).
Sotirchos, S. V., and H. C. Yu, "Overlapping Grain Models for Gas-Solid Systems with Solid Product," *Ind. Eng. Chem. Res.*, **27**, 836 (1988).
Sotirchos, S. V., and S. Zarkanitis, "A Distributed Pore Size and Length Model for Porous Media Reacting with Diminishing Porosity," *Chem. Eng. Sci.*, **48**, 1487 (1993).
Szekely, J., and J. W. Evans, "A Structural Model for Gas-Solid Reactions with a Moving Boundary: II. The Effect of Grain Size, Porosity and Temperature on the Reaction of Porous Pellets," *Chem. Eng. Sci.*, **26**, 1901 (1971).
Szekely, J., J. W. Evans, and H. Y. Sohn, *Gas-Solid Reactions*, Academic Press (1976).
Ulerich, N. H., E. P. O'Neill, and D. L. Keairns, "The Influence of Limestone Calcination on the Utilization of Sulfur Solvent in Atmospheric Pressure Fluid-Bed Combustors," EPRI FP-426 (1977).
Wakao, N., and J. M. Smith, "Diffusion in Catalyst Pellets," *Chem. Eng. Sci.*, **17**, 825 (1962).
Wang, W., Q. Zhong, Z. Ye, and I. Bjerle, "Simultaneous Reduction of SO_2 and NO_x in an Entrained Flow Reactor," *Fuel*, **74**, 267 (1995).
Wen, C. Y., and M. Ishida, "Reaction Rate of Sulfur Dioxide with Particles Containing Calcium Oxide," *Environ. Sci. Technol.*, **7**, 703 (1973).
Ye, Z., W. Wang, Q. Zhong, and I. Bjerle, "High Temperature Desulfurization Using Fine Sorbent Particles under Boiler Injection Conditions," *Fuel*, **74**, 743 (1995).

Appendix

The unsteady-state diffusion of the ions through the product sulfate layer in the subgrain can be given by the following differential equation

$$D_{\text{ion}} \frac{1}{r^2} \frac{\partial}{\partial r}\left(r^2 \frac{\partial C_{\text{ion}}}{\partial r} \right) = \frac{\partial C_{\text{ion}}}{\partial t} \tag{A1}$$

subject to the boundary conditions

$$C_{\text{ion}}|_{r=r_c} = \rho_{\text{CaO}} \tag{A2}$$

$$-D_{\text{ion}} \left(\frac{\partial C_{\text{ion}}}{\partial r} \right)\Bigg|_{r=r_g} = k_s C_{\text{ion}} C_{\text{SO}_2} \tag{A3}$$

As no analytical solution is available for this equation (subject to these boundary conditions) and numerical solutions encounter severe "stiffness" problems, an appropriate solution can be obtained by assuming pseudo-steady state. In order to justify this assumption a comparison between unsteady state and the pseudo-steady state is made on the basis of the perturbation solution given by Bowen (1965). The sulfur dioxide concentration at the surface of a subgrain C_{SO_2} is assumed constant for the purpose of comparison. Therefore, Eq. A3 reduces to

$$-D_{\text{ion}} \left(\frac{\partial C_{\text{ion}}}{\partial r} \right)\Bigg|_{r=r_g} = k'_s C_{\text{ion}} \tag{A4}$$

where

$$k'_s = k_s C_{SO_2} \tag{A5}$$

A perturbation solution for these equations is given by Bowen (1965), which involves a parameter λ, given by

$$\lambda \equiv \frac{\tau_D}{\tau_C} = \frac{r_g k'_s}{D_{ion}} \tag{A6}$$

where τ_D ($\equiv r_g^2/D_{ion}$) and τ_C ($\equiv r_g/k'_s$) are the characteristic times for diffusion and chemical reaction.

Bowen (1965) has shown that when $\lambda < 1$, diffusion times are short when compared to reaction times, and the pseudo-steady-state approximation can be applied to Eqs. A1 through A4.

Taking the representative values of the corresponding parameters for the diffusion of Ca^{2+} ions through the $CaSO_4$ product layer for CaO sulfation, we obtain: $r_g = 1 \times 10^{-7}$ m; $k'_s = 1 \times 10^{-10}$ m/s; and $D_{ion} = 1 \times 10^{-16}$ m^2/s. Substituting these values in Eq. A6 yields a value for λ of 0.1.

Manuscript received June 1, 1998, and revision received Dec. 7, 1998.